Accepted Manuscript

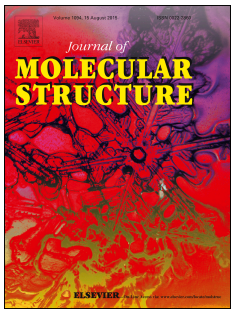

Synthesis, Crystal Structure, Hirshfeld Surface Analysis and DNA Binding Studies of 1-((E)-3-(4-bromophenyl)-1-phenylallylidene)-2-(m-tolyl)hydrazine

Rabail Ujan, Nasima Arshad, Aamer Saeed, Pervaiz Ali Channar, Shahid Iqbal Farooqi, Parvez Ali Mahesar, Fayaz Ali Larik, Mahboob Ali Rind, Tuncer Hökelek, Ulrich Flörke

PII: S0022-2860(19)30420-X

DOI: https://doi.org/10.1016/j.molstruc.2019.04.025

Reference: MOLSTR 26397

To appear in: *Journal of Molecular Structure*

Received Date: 7 February 2019

Revised Date: 3 April 2019

Accepted Date: 5 April 2019

Please cite this article as: R. Ujan, N. Arshad, A. Saeed, P.A. Channar, S.I. Farooqi, P.A. Mahesar, F.A. Larik, M.A. Rind, T. Hökelek, U. Flörke, Synthesis, Crystal Structure, Hirshfeld Surface Analysis and DNA Binding Studies of 1-((E)-3-(4-bromophenyl)-1-phenylallylidene)-2-(m-tolyl)hydrazine, *Journal of Molecular Structure*, https://doi.org/10.1016/j.molstruc.2019.04.025.

Graphical abstract:

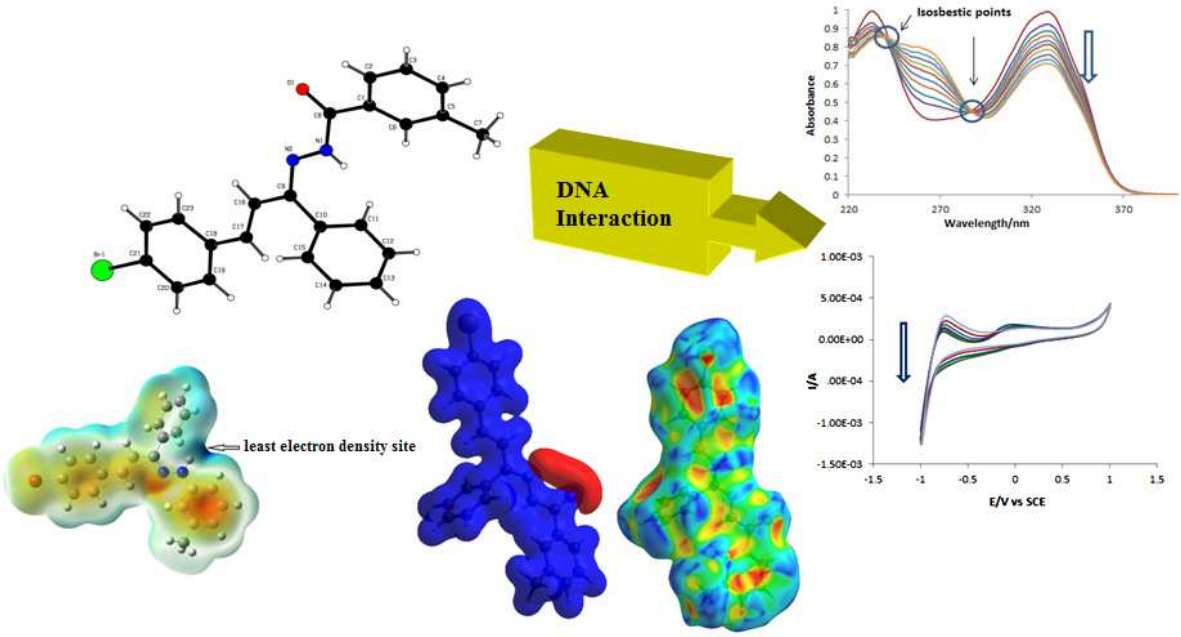

A new compound 1-((E)-3-(4-bromophenyl) -1-phenylallylidene)-2-(m-tolyl)hydrazine was synthesized and studied for X-ray, Hirshfeld surfaces, DFT and DNA binding analysis.

Highlights:

- 1-((E)-3-(4-bromophenyl) -1-phenylallylidene)-2-(m-tolyl)hydrazine - A new chalcone Schiff base
- Crystal structure determination
- Hirshfeld surface analysis
- DFT and experimental studies for DNA binding

Synthesis, Crystal Structure, Hirshfeld Surface Analysis and DNA Binding Studies of 1-((E)-3-(4-bromophenyl)-1-phenylallylidene)-2-(m-tolyl)hydrazine

Rabail Ujan [a], Nasima Arshad [b,*], Aamer Saeed [c,*], Pervaiz Ali Channar [c], Shahid Iqbal Farooqi [b], Parvez Ali Mahesar [d], Fayaz Ali Larik [c], Mahboob Ali Rind [a], Tuncer Hökelek [e], Ulrich Flörke [f]

[a] *M. A. Kazi Institute of Chemistry, University of Sindh, Jamshoro -76080, Pakistan*

[b] *Department of Chemistry Allama Iqbal Open University-44000, Islamabad, Pakistan*

[c] *Department of Chemistry Quaid-i-Azam University-45320, Islamabad, Pakistan*

[d] *Institute of Chemistry, Shah Abdul Latif University, Khairpur- 66020, Pakistan*

[e] *Department of Physics, Faculty of Engineering, Hacettepe University-06800 Beytepe-Ankara, Turkey*

[f] *Department Chemie, Fakultätfür Naturwissenschaften, Universität Paderborn, Warburgerstrasse -100, 33098 Paderborn, Germany*

---

[*] **Corresponding author;**

Email: nasimaa2006@yahoo.com; nasima.arshad@aiou.edu.pk

Phone: +92-51-905-7756

Co-corresponding author;

E mail: aamersaeed@yahoo.com

Tel: +92-51-9064-2128

Abstract

1-((E)-3-(4-bromophenyl) -1-phenylallylidene)-2-(m-tolyl)hydrazine (**4**) was synthesized and characterized for structural elucidation by spectroscopy (FT-IR, ^{1}H-NMR, and ^{13}C-NMR) and single crystal X-ray diffraction. In the title compound, the benzene rings A, B, C were oriented at dihedral angles {A/B = 82.92(3)°, A/C = 24.12(3)°and B/C = 75.90(3)°}. Crystal structure showed that intermolecular C—H···O and C—H···N hydrogen bonds linked the molecules, enclosing R_2^2 (10) and R_2^2 (16) ring motifs. The Hirshfeld surface analysis of the crystal structure indicated that the most important contributions for the crystal packing were from H···H (46.0%), H···C/C···H (17.6%), H···Br/Br···H (12.4%), H···O/O···H (8.5%) and C···C (6.6%) interactions. Hydrogen bonding and van der Waals contacts were the dominant interactions in the crystal packing. Compound's interaction with DNA was further investigated theoretically by DFT and experimentally by UV-visible spectroscopy and cyclic voltammetry. DFT analysis in terms of geometry optimization and computed parameters revealed reactive nature of **4** and the possibility of planar phenyl rings to intercalate within the DNA base pairs. Spectral and voltammetric analysis and related binding parameters suggested intercalation as a possible mode for **4** – DNA binding which was further verified by viscosity measurements.

Keywords: Chalcone Schiff base, X-ray single crystal, Hirshfeld surface analysis, DFT studies, DNA binding by UV & CV, Viscosity measurement

1. Introduction

α-β-unsaturated ketones are commonly known as chalcones; this class of compounds had exhibited diverse biological activates. Most importantly, anti-HIV, anti-cancer, anti-viral, anti-

inflammatory, anti-fungal, anti-oxidant, anti-convulsant, anti-hypertensive, anti-filarial, antiprotozoal, anti-bacterial and anti-malarial activities have been reported in recent literature [1]. Following important compounds of same nature are illustrated, as anti-cancer **1**, anti-malarial **2**, anti-bacterial **3**, anti-inflammatory **4**, anti-protozoal **5**, anti-HIV **6**, in Fig.1, [2-7]. The different methods of chalcones' synthesis and their derivatives were reported in the literature [8-11]. Thiosemicarbazones are formed due to the condensation reaction between aldehyde or ketone with thiosemicarbazide [12]. This class has already been taken numerous attentions of the world due to a broad category of biological activities such as Marboran **7** exhibit antiviral [13], menthone thiosemicarbazone **8** possesses anti-HIV and **9** contain the broad-spectrum anticancer activity [14,15], Fig. 1. Such α-β-unsaturated ketone based thiosemicarbazone is a novel skeleton and a new entry to organic compounds and possessing some important biological activities.

In the body; DNA damaging occurs mainly due to oxidative stress and exposure to the toxic environment. Many abnormal changes in the DNA could lead to genomic instability and mutation that may further be resulted in several types of cancers [16, 17]. Although the drugs available in the market prohibit the proliferation process which causes the death of cancer cells; most of them have severe side effects on healthy organs of a body [18].

Among non-covalent and covalent binding of a drug with the DNA; the later one mode results in the irreversible contact of the compound with DNA which also harms the healthy cell [19-21]. However, non-covalent binding is a reversible type binding and is considered comparatively safer with less or no side effect. A compound could bind reversibly with DNA via intercalation between the DNA base pairs, electrostatic interactions and via major/or minor grooves. So an effort to investigate and design a drug with minimal side effects is continuously a

focus of interest of chemical, biological and pharmacological researchers [21, 22]. In this respect, several new compounds have been explored, by in vitro experimental and theoretical studies for reversible DNA binding interactions, to probe their potency as therapeutic agents [23-29].

In this paper, we are reporting a novel single crystal 1-((E)-3-(4-bromophenyl) -1-phenylallylidene)-2-(m-tolyl)hydrazine (**4**) for crystal structure analysis and intermolecular interactions. The compound was further investigated for its binding with DNA.

Fig.1

2. Experimental Section

2.1. Material and methods

All chemicals and reagents used in experimental work are of analytical grade. Solvent purification and drying were done using standard methods and stored over molecular sieves. For monitoring of the synthetic reactions; thin layer chromatography (TLC) was conducted on 0.25 mm silica gel plates (60 F254, Merck). Visualization of chromatogram was made under UV-lamp at 365 and 254 nm. R_f value was calculated using a solvent system of petroleum ether: ethyl acetate in 4:1 ratio. The yield (%) given was on the basis of 1.0 mM of each precursor used. Falcon protocol was used for the extraction of double-strand (ds) DNA from calf thymus (ct-DNA) gland. Double distilled autoclaved water and autoclaved apparatus were used in total extraction procedure. DNA threads were collected by using a glass hook and dissolved in autoclaved water. A stock solution of DNA was further diluted and its purity was monitored by using UV-visible spectrophotometer. The absorbance ratio of ct-DNA at A_{260}/A_{280} was evaluated in between 1.8 – 1.9, which assured its sufficient purity with no protein contamination [29]. The

DNA concentration was determined by using the value of molar extinction coefficient ε_{260} = 6600 cm^{-1} M^{-1} in Beer's law. The stock solution of the compound **4** was prepared in 50% buffered ethanol having pH 4.7. The concentration of **4** was optimized to 3.45 × 10^{-4} M for all DNA binding investigations.

2.2. Instrumentations

Melting points were recorded using a digital Gallenkamp (SANYO) model MPD.BM 3.5 apparatus and are uncorrected. ^{1}H-NMR and ^{13}C-NMR spectra were determined at 300 MHz using a Bruker AM-300 spectrophotometer. FTIR spectra were recorded on a Bio-Rad-Excalibur Series Mode FTS 3000 MX spectrophotometer. Mass Spectra (EI, 70eV) on a GC-MS, Agilent Technologies 6890N elemental analyses were conducted using a LECO-183 CHNS analyzer. A Vortex machine and Hettich EBA20 Portable Centrifuge C 2002 having maximum speed up to 6000 per minute were used during the ct-DNA extraction procedure. Temperature controller Shimadzu 1800 spectrophotometer having 1 cm quartz cells and AUTOLAB PGSTAT-302 potentiostat/galvanostat with the electrochemical software package GPES version 4.9 (Eco Chemie, Utrecht, Netherlands) was used for DNA binding experiments. Dr. Bob cell (double walled; 1-30 mL capacity) was used for electrochemical experiment and attached to water circulating bath to achieve the required temperature of the samples within the cell. The cell was prepared by dipping into the sample solution a glassy carbon (GCE; d = 3 mm), saturated calomel (SCE; 3.5 M KCl) and a Pt wire as working, reference and counter electrode, respectively. In order to avoid the ohmic drop; a reference electrode was placed in lugging capillary which provides proper sensing point for the reference electrode near the working electrode. The glassy carbon electrode was polished with α-alumina powder, washed,

ultrasonicated for 30 seconds and dried before used. An automated Schott Gerate viscometer (Model; AVS 310) was used in viscometric experiments.

2.3. General procedure for the synthesis

*2.3.1. Synthesis of (E)-3-(4-bromophenyl)-1-phenylprop-2-en-1-one **(3)***

The Chalcone (*E*)-3-(4-bromophenyl)-1-phenylprop-2-en-1-one (**3**) was synthesized by base catalyzed Claisen-Schmidt condensation reaction of acetophenone and 4-bromobenzaldehyde by the known literature method [30]. Thus, a mixture of 4-bromobenzaldehyde (**1**) (0.01 mol) and acetophenone (**2**) (0.01 mol) was dissolved in 10 ml ethanol in a 250 ml round-bottomed flask equipped with a reflux condenser. To the stirred reaction mixture, 10 ml NaOH solution (1g in 10 ml H_2O) was added dropwise while the reaction temperature was maintained between 20-25 ^oC. After vigorous stirring for 4 hours, the reaction mixture was neutralized by 0.2 N HCl whereby the precipitation occurred. On filtration, the solid obtained was recrystallized from aqueous ethanol to afford chalcone (**3**) as colorless crystals.

*2.3.2. 1-((E)-3-(4-bromophenyl)-1-phenylallylidene)-2-(m-tolyl)hydrazine **(4)***

1-((E)-3-(4-bromophenyl)-1-phenylallylidene)-2-(m-tolyl)hydrazine (**4)** was synthesized in the laboratory by reflux method. 3-methylbenzohydrazide (0.5g, 3.65 mmol) was dissolved in 15ml of absolute alcohol. (E)-3-(4-bromophenyl)-1-phenylprop-2-en-1-one (3.70 mmol) was added with constant stirring in the presence of catalytic amount of acetic acid. The reaction mixture was refluxed for 4-6 hours and the completion of the reaction was monitored by TLC (petroleum ether; ethyl acetate 4:1). The reaction mixture was cooled and the resulting solid was

filtered, washed with cold ethanol and finally recrystallized from aqueous ethanol to afford (**4**) as yellowish crystals.

*2.4. Characterization data of **4***

Yield:70%: m.p 268°C R_f: 0.57; Petroleum ether : ethylacetate (4:1) FTIR; (KBr, cm^{-1}): 3348 (NH), 3189 (sp^2CH), 1646 (C=N), 1540 (Ar-C=C), ^{1}H NMR (300 MHz, DMSO-d_6): δ (ppm): 11.1 (s, 1H, NH), 7.42 (d, 2H, ArH), 7.19 (d, 2H, ArH), 6.75-7.41 (m, ,4H Ar-H), 7.20-6.91 (m, 5H, Ar-H); 7.25 (d -CH=CH-) 6.50 (d -CH=CH-) 2.51 (s, 3H, CH_3); ^{13}C NMR (75 MHz, DMSO-d_6): δ (ppm):. 158.4 (C=N), 143.9, 141.3, 138.6, 137.9, 134.5, 133.2, 132.5, 130.2, 129.8, 129.0, 128.5, 125.4, 122.4, 120.5, 116.8, 113.5, 22.5. Anal. Calcd. For $C_{22}H_{19}BrN_2$ C, 67.53; H, 4.89; N, 7.16 Found: C, 67.50; H, 4.82; N, 7.14.

2.5. Crystal structure determination and refinement

The intensity data were recorded using a Bruker AXS SMART APEX CCD area-detector diffractometer with graphite monochromated MoK_α radiation (λ = 0.71073 Å) at T = 130(2) K. Direct methods were employed to solve the structure and its refinement was done by full-matrix least squares against F^2 [31, 32]. All non H-atoms were refined anisotropically. Hydrogen atoms were clearly located in a difference Fourier maps and then refined at idealized positions riding on the carbon atoms with isotropic displacement parameters $U_{iso}(H) = 1.2U_{eq}(C)$ or $1.5U_{eq}$ (-CH_3) & (C-H) 0.95-0.98 Å, H(N) was refined freely. All CH_3 hydrogen atoms were allowed to rotate but not to tip. Crystallographic data for the structure reported in this paper have been deposited with the Cambridge Crystallographic Data Centre as supplementary publication no. CCDC-1831398. Copies of available material can be obtained free of charge via www.ccdc.cam.ac.uk.

2.6. Hirshfeld surface calculations

Crystal Explorer program 17.5 was employed to carry out the Hirshfeld surface analysis [33]. The structural input file was obtained in the CIF format. Hirshfeld surface distance from the nearest nucleus inside and outside the surface was measured and represented by d_i and d_e, respectively, while a normalized contact distance was represented as d_{norm}. White, red and blue colors have been selected for the visualization of d_{norm}.

2.7. DFT calculations

Theoretical DFT analysis of **4** for its structure and reactivity was done by using Gaussian 09 software at DFT/ B3LYP/ basis set (6-31G) level. The geometry of **4** was optimized and quantum parameters were computed.

2.8. DNA binding experiments

DNA binding experiments for **4** at UV- visible spectrophotometer and an electrochemical instrument were run by adjusting the temperature of sample holders of both instruments (cell cuvette & Dr. Bob cell) at 37^{o}C. Initially, the compound at its fixed concentration was run separately for UV- and CV and then titrations were performed with DNA concentrations under physiological pH (Stomach; 4.7) and temperature (37^{o}C). During titration experiments, ct-DNA was added gradually from 10 – 90 µM into the solution of **4 (**3.45×10^{-4} M). Before starting next titration; sample solution was allowed to stay for a few minutes so that an equilibrium between compound and DNA could be achieved. For UV- visible experiments wavelength was adjusted within the range of 200 – 400 nm, while the potential range of +1.5 – -1.5 V was used in CV

experiments. In order to avoid oxygen in the sample solution, bubbling for 10 – 15 minutes and jacketing of argon gas (99.999% pure) was done before each CV experiment. The scan rate was adjusted to 100 mV/s. Conversely, in viscosity experiments, DNA concentration was kept constant to 10 μM and the compound was added gradually in its increasing concentration from (10 – 80 μM).

3. Results and Discussion

3.1. Chemistry

The synthesis of target Schiff base **4** was carried out according to Scheme 1. 3-methylbenzohydrazide in dry ethanol was allowed to react with (*E*)-3-(4-bromophenyl)-1-phenylprop-2-en-1-one in the presence of acetic acid as catalyst, to obtain the desired compound (**4**) in good yield. The compound obtained was purified by recrystallization from aqueous ethanol. The appearance of C=N at 1646 cm^{-1}, Ar-C=C at 1540 cm^{-1} and stretching around 3348 cm^{-1} indicated the presence of NH moiety in the title compound. In ^{1}H NMR spectrum, the appearance of a singlet at 11.1 was noticed for NH. The characteristic of alkene protons was observed in the range of 7.25 – 6.50 ppm in ^{1}H NMR spectra. In ^{13}C NMR spectra, the signals at 158.4 (C=N) confirmed the formation of the **4 {**1-((E)-3-(4-bromophenyl)-1-phenylallylidene) -2-(m-tolyl) hydrazine}.

Scheme 1

3.2. Description of the crystal structure

The single crystal X-ray structural determination of the title compound confirms the assignment of its structure from spectroscopic data. The experimental details including the

crystal data, data collection and refinement are summarized in Table 1. The hydrogen-bond geometry, the selected interatomic distances, and the selected bond lengths, bond angles together with the torsion angles are given in Tables 2, 3 and 4, respectively. The molecular structure along with the atom-numbering scheme is depicted in Fig. 2. Atoms C7, C8, C9, C17, and Br1 are 0.0660(3), 0.0347(3), -0.0650(2), 0.0501(3) and 0.0491(3) Å away from the mean planes of the adjacent benzene rings A (C1-C6), B (C10-C15) and C (C18-C23), respectively. So, atoms C7 and C8, C9, and C17 and Br1 are co-planar with the adjacent benzene rings A, B, and C, respectively. The benzene rings, A, B, and C, are oriented at dihedral angles of A/B = 82.92(3)°, A/C = 24.12(3)° and B/C = 75.90(3)°.

In the crystal structure, intermolecular C—H ··· O and C—H ··· N hydrogen bonds (Table 2) link the molecules into infinite chains, enclosing R_2^2 (10) and R_2^2 (16) ring motifs, Fig. 3, [34]. Hydrogen bonding and van der Waals contacts are the dominant interactions in the crystal packing. No significant π ··· π and C—H ··· π interactions are observed.

Table 1 – 4, Fig. 2&3

3.3. Hirshfeld surface analysis

In order to visualize the intermolecular interactions in the crystal of the title compound; Hirshfeld surface (HS) analysis is carried out to investigate the locations of atoms ···atom short contacts with potential to form hydrogen bonds and the quantitative ratios of these interactions besides of the π-stacking interactions [35-37]. The normalized contact distance, d_{norm}, enable the identification of the regions of particular importance to intermolecular interactions. In the HS plotted over d_{norm}, Fig. 4, the white surface indicated contacts with distances equal to the sum of van der Waals radii, and the red and blue colors indicate distances shorter (in close contact) or longer (distinct contact) than the van der Waals radii, respectively [38]. The bright-red spots

appearing near O1, N2 and hydrogen atoms H1*A* and H15*A* indicate their roles as the respective donors and acceptors in the dominant C–H ⋯ N and C–H ⋯ O hydrogen bonds; they also appear as blue and red regions, respectively, corresponding to positive and negative potentials on the HS mapped over electrostatic potential as shown in Fig. 5, [37, 39]. The blue regions indicate the positive electrostatic potential (hydrogen-bond donors), while the red regions indicate the negative electrostatic potential (hydrogen-bond acceptors).

The shape-index of the HS is a tool to visualize the π ⋯ π stacking by the presence of adjacent red and blue triangles; if there are no adjacent red and/or blue triangles, then there are no π ⋯ π interactions. Fig. 6 clearly suggests that there are no π ⋯ π interactions in the title compound. The intermolecular interactions present in the structure are also visible on the two-dimensional fingerprint plot, where one molecule acts as a donor, $d_e > d_i$, and the other as an acceptor, $d_i > d_e$. The combination of d_e and d_i in the form of a two-dimensional fingerprint plot provides a summary of the intermolecular contacts in the crystal. The overall two-dimensional fingerprint plot, Fig. 6*a* and those delineated into H···H, H···C/C···H, H···Br/Br···H, H···O/O···H, C···C, H···N/N···H, N···C/C···N and C…Br/Br…C contacts [40] are illustrated in Figs. 6 *b-i*, respectively, together with their relative contributions to the Hirshfeld surface. In the fingerprint plot delineated into H···H contacts Fig. 6*b*, the 46.0% contribution to the HS is viewed as widely scattered points of high density due to the large hydrogen content of the molecule. The single spike with the tip at $d_e = d_i \sim 1.07$ Å is due to the short interatomic H···H contacts, Table 3.

In the absence of C–H ⋯ π interactions in the crystal, the forceps-like pair of characteristic wings resulting in the fingerprint plot delineated into H···C/C···H contacts, Fig. 7*c*, have an asymmetric distribution of points, where C···H interactions have a larger contribution (10.2%) than their H···C counterparts (7.4%). Thus, the sum of H···C/C···H interactions has a 17.6%

contribution to the total HS area of the molecule and is viewed with the tips at $d_e + d_i \sim 2.66$ Å result from short interatomic H···C/C···H contacts (Table 3). In the fingerprint plot delineated into H···Br/Br···H contacts in the structure with 12.4% contribution to the HS have also an asymmetric distribution of points Fig. 7*d*, where Br···H interactions have a larger contribution (8.1%) than their H···Br counterparts (4.3%), and are viewed as distinct pair of spikes with the tips at $d_e + d_i \sim 2.91$ Å result from short interatomic H···Br/Br···H contacts (Table 3). The symmetrical distribution of points in the fingerprint plot delineated into H···O/O···H contacts, Fig. 7*e*, the 8.5% contribution to the overall crystal packing is viewed as a pair of spikes with the tips at $d_e + d_i \sim 2.34$ Å result from short interatomic H···O/O···H contacts, Table 3. In the fingerprint plot delineated into C··· C contacts, Fig. 7*f*, the 6.6% contribution to the HS arises from the interatomic C···C contacts listed in Table 3, and is viewed as a spoon-like spike with the tip at $d_e = d_i \sim 1.77$ Å. The symmetrical distributions of points in the fingerprint plots delineated into H···N/N···H (Figs. 7*g*) and N···C/C···N (Figs. 7*h*) contacts, the 3.1% contributions to the overall crystal packing are viewed as pairs of spikes with the tips at $d_e + d_i \sim 2.40$ Å (for H···N/N···H contacts) and $d_e + d_i \sim 3.21$ Å (for N···C/C···N contacts) result from short interatomic H···N/N···H and N···C/C···N contacts (Table 3). Finally, the symmetrical distribution of points in the fingerprint plot delineated into C···Br/Br···C contacts, Fig. 7*i*, the 2.4% contribution to the overall crystal packing is viewed as a pair of spikes with the tips at $d_e + d_i \sim 3.54$ Å result from short interatomic C···Br/Br···C contacts (Table 3).

The individual intermolecular interactions, together with their quantitative contributions, described above can also be visualized by the different Hirshfeld surface representations with the function d_{norm} plotted onto the surface, and they are shown for H···H, H···C/C···H, H···Br/Br···H, H···O/O···H, C···C, H···N/N···H, N···C/C···N and C···Br/Br···C interactions in Fig. 8 *a*—*h*,

confirming that the Hirshfeld surface analysis provides a full understanding of the intermolecular interactions in a facile and immediate way.

The Hirshfeld surface analysis confirms the importance of H-atom contacts in establishing the packing. The large number of H···H, H···O/O···H and H···C/C···H interactions suggest that van der Waals interactions and hydrogen bonding play the major roles in the crystal packing [41] .

Fig. 4 - 8

3.4. Computational DFT studies

DFT computational analysis is considered the most reliable for theoretical investigations on compound's reactivity and the binding possibilities for the compound's interaction with DNA. The optimized geometry, an electrostatic potential map for a maximum charge distribution and HOMO-LUMO orbitals of the title compound are given in Fig. 9 and computed parameters are provided in Table 5. Optimized structure indicated the presence of two phenylene rings and one phenyl ring; hence **4** showed the possibility that it could intercalate through insertion /intercalation of these planar rings into the DNA base pairs. Least electron density site in electrostatic potential map indicated the most electron deficient hydrogen which can accept the lone pair of electrons from the electron rich parts of bases i.e., NH_2, NH, =O etc of the DNA. This caused hydrogen bonding which resulted in the stability of **4** – DNA adduct.

Stability, polarizability and the binding tendency of a compound could be justified on the basis of computed ΔE (HOMO – LUMO energy gap). The evaluated ΔE value for **4** was found very small, Table 5, which indicated that the compound is unstable and hence reactive in nature. A high negative value of binding energy, the greater value of dipole moment and a small value of

hardness, as presented in Table 5, further authenticated instability and greater tendency **4** towards binding with DNA [28].

Fig. 9, Table 5

3.5. DNA-binding studies by UV- visible spectroscopy

DNA binding studies are considered the most significant way to investigate the binding potentials of compounds that could act as anti-cancer drugs. UV- visible spectroscopy is the most frequently employed and appropriate technique for DNA binding analysis of compounds.

Initially, UV- visible spectrum of **4** was run at its fixed concentration of 3.45×10^{-4} M under physiological conditions (pH 4.7; Temp. 37 ^{o}C) and shown in Fig. 10 (left; the topmost spectrum). Two absorbance peaks appeared in the spectrum of **4**; one with λ_{max} of 226 nm and the other with λ_{max} of 327 nm. The peaks at higher and lower wavelengths could be designated to appear due to low energetic $\pi \cdots \pi$ and high energetic $n \cdots \pi^*$ transitions, respectively. Then, compound's spectra were recorded in the presence of varying ct-DNA concentrations, Fig.10 (left; along the arrow direction). Upon addition of DNA from 10 – 90 µM into the sample solution; a prominent hyporchromism was observed along with redshift. The % drop in the absorbance peak was evaluated 34.5 % while peak shift towards longer wavelength was found 3.5 nm. This pronounced hypochromic effect with bathochromic (red) shift as well as planarity in the compound's structure clearly indicated that the **4** – DNA interaction has occurred via intercalation of **4** into the DNA base pairs [42]. Further, two isosbestic points also appeared in the UV-visible spectra which showed that an equilibrium

mixture of **4** and DNA was present in the sample; hence the possibility of species other than **4** and DNA could be ignored.

Benesi-Hildebrand and classical Van't Hoff's equation was used to calculate the intrinsic binding constant (K_b) and Gibbs free energy change (ΔG), respectively [23-29].

$$\frac{A_o}{A - A_o} = \frac{\varepsilon_G}{\varepsilon_{H-G} - \varepsilon_G} + \frac{\varepsilon_G}{\varepsilon_{H-G} - \varepsilon_G} \frac{1}{K_b [DNA]} \quad (1)$$

$$\Delta G = -RT \ln K_b \quad (2)$$

Where, A_o and A are compound's absorption in the absence and presence of ct-DNA, respectively; ε_G and $\varepsilon_{H\text{-}G}$ are molar extinction coefficient of pure compound and compound – DNA bound complex, respectively. By plotting $A_o/A\text{-}A_o$ vs.1/[DNA], the value of binding constant K_b was obtained from the intercept to slope ratio, Fig. 2 (right). The calculated value of the binding constant was found to 4.1×10^3 M^{-1}. By using the value of K_b in Eq. 2; free energy change (ΔG) was evaluated and the value was found to -21.44 kJ mol^{-1}, which showed spontaneity in the **4** – DNA binding.

Fig.10

3.6. DNA binding studies by cyclic voltammetry

Cyclic voltammetry is a technique that has gained the parallel importance as UV-visible spectroscopy for DNA binding studies. Experimental results obtained from both techniques are helpful to elucidate kinetic and thermodynamic parameters. These parameters together with instrumental responses are quite informative to investigate compound–DNA binding.

The cyclic voltammetric experiments were run on a glassy carbon electrode within the potential scan range of -1.5 – 1.5 V and a scan rate of 100 mV/s. In 50% buffered ethanol (pH

4.7); compound's voltammograms were scanned at 37°C without and in the presence of varying DNA concentrations (10 – 50 μM) and shown in Fig.11 (left). The voltammogram of **4** showed two irreversible reduction peaks at -0.772 V and -0.048V. Significant changes in the electrochemical responses of **4** after the addition of varying DNA concentrations was only observed for a peak at a more negative potential. Upon DNA additions; a gradual decrease in peak current was observed along with the peak shift towards less negative potential. The magnitude of the current drop was evaluated 22.7% which showed that the concentration of free compound has decreased. On the other hand, **4** have interacted with DNA via formation of the compound – DNA complex.

Variation in current responses was further used in the following equation to determine the binding constant of **4** after DNA interaction [23-29, 43].

$$I_p^2 = \frac{1}{K_b[DNA]}(I_{po}^2 - I_p^2) + I_{po}^2 - [DNA] \quad (3)$$

In the equation, I_{po} and I_p represent peak current of **4** alone and after DNA addition, respectively. A plot of I_p^2 vs. I_{po}^2- I_p^2/ [DNA] gave a straight line with a slope equal to the reciprocal of binding constant, K_b, Fig.11 (right). The binding constant of compound–DNA complex was calculated to be 5.62×10^3 M^{-1} while using K_b value in Eq. 2; ΔG was evaluated to -22.25 kJ mol^{-1}.

The K_b value was found in 1000th order of magnitude with both UV and CV studies and the same order has been reported for an intercalator isoxazocucumine (6.3×10^3 M^{-1}) [43]; hence on the basis of structure, spectral / voltammetric responses and binding data; the investigated compound could be predicted to have affinity with DNA via intercalation into its base pairs.

Fig.11

3.7. Viscometric studies

The more comprehensive and simple way to verify the binding of a compound with DNA is to measure the viscosity of DNA after the addition of compound's concentrations. DNA lengthening is resulted due to insertion of a compound's planar portions into the base pairs; as a result, enhancement in the viscosity of DNA solution is observed. Hence this method could act as a verification tool for DNA binding studies. The viscosity of DNA fixed concentration (10 μM) before and after the addition of varying concentrations of **4** (10 – 80 μM) was measured. A graph was plotted between relative specific viscosity $(\eta/\eta_o)^{1/3}$ vs. [compound]/[DNA] concentration ratio and showed a linear rise in the relative specific viscosity of DNA in the presence of **4**, Fig. 12. The observed change in DNA viscosity is an indication that **4** has bound with DNA via insertion of phenyl rings between the base pairs of DNA. This increase in the viscosity not only indicated intercalative binding but it also authenticated the hypochromism and redshift observed in UV- visible spectroscopy [23, 44].

Fig.12

4. Conclusions

A novel Schiff base- 1-((E)-3-(4-bromophenyl) -1-phenylallylidene)-2-(m-tolyl)hydrazine (**4**) was synthesized and characterized by spectroscopic techniques. Single crystal X-ray structure determination of the title compound was confirmed by assignment of its structure from spectroscopic data and clarified in detail. Intermolecular close contacts in the crystal structure of **4** by Hirshfeld surface analysis were visualized and quantified. HS analysis showed excessive H···H, H···C/C···H, H···Br/Br···H, H···O/O···H and C···C interactions which confirmed the major role of van der Waals and hydrogen bonding in the crystal packing. Geometry optimization and

quantum parameters by DFT analysis revealed the reactive nature of **4** and the possibility for its binding with DNA. Responses and data analysis by both spectroscopic and voltammetric experiments were complimentary and indicated that **4** could interact with DNA base pairs via insertion into the DNA duplex. Enhancement in the viscosity of DNA solution in the presence of **4** justified the theoretical and experimental findings and further disclosed that the test compound has a tendency to bind with DNA via intercalation. However, some more in-vivo/vitro experiments in biology and pharmaceutics may be needed for further verification of **4** as a potential anticancer drug agent.

Acknowledgments

The authors would like to thanks all the mentioned departments of national and international universities/institutes for the accomplishment of research explored in this paper.

Conflicts of Interest

Authors declare no conflict of interest.

References

1. P. Singh, A. Anand, V. Kumar, *Eur. J. Med. Chem.***2014,**85, 758–777.
2. B.P. Bandgar, S.S. Gawande, R.G. Bodade, J.V. Totre, C.N. Khobragade, *Bioorg. Med. Chem.* **2010**, 18, 1364–1370.
3. N. Yadav, S.K. Dixit, A. Bhattacharya, L.C. Mishra, M. Sharma, S.K. Awasthi, V.K. Bhasin *Biol. Drug Des.***2012,**80, 340–347.

4. M. Subramanian, G. Vanangamudi, G. Thirunarayanan, *Spectrochim. Acta A: Mol. Biomol. Spectrosc*. **2013,**110, 116–123.

5. S. Bano, K. Javed, S. Ahmad, I.G. Rathish, S. Singh, M. Chaitanya, K.M. Arunasree, M.S. Alam, *Eur. J. Med. Chem.***2013,**65, 51–59

6. S.A.Carvalho, L.O.Feitosa, M**.** Soares, T.E.M.M.Costa, M.G.Henriques, K.Salomao, S.L.D.Castro, M.Kaiser, R.Brun, J.L.Wardell, S.M.S.V.Wardell, G.H.G.Trossini, Andricopulo, E.F.D.Silva, C.A.M.Fraga, *Eur. J. Med. Chem.*2012, 54, 12–522.

7.H. Sharma, S. Patil, T.W. Sanchez, N. Neamati, R.F. Schinazi, J.K. Buolamwini, *Bioorg. Med. Chem.* **2011**, 19, 2030–2045.

8.A. Guida, M.H. Lhouty, D. Tichit, F Figueras, P. Geneste, *Appl. Catal. A: Gen*. **1997,**164 , 251–264.

9. G. Romanelli, G. Pasquale, Á. Sathicq, H. Thomas, J. Autino, P. Vázquez, *J. Mol.Catal. A: Chem.***2011,**340, 24–32

10. S. Eddarir, N. Cotelle, Y. Bakkour, C. Rolando, Tetrahedron Lett. **2003,**44, (28)5359–5363.

11. D.N. Dhar, The chemistry of chalcones and related compounds. John Wiley & Sons. **1981**

12. J.S. Casas, M.S. Garcıa-Tasende, J. Sordo, *Coord. Chem. Rev.***2000,**209 (1)197–261.

13. C. Debra Quenelle , A. Kathy Keith, R. Earl Kern. / Antiviral Research 71 (2006) 24–30

14. V. Mishra, S.N. Pandeya, C. Pannecouque, M. Witvrouw, E. De Clercq,. *Arch. Pharm. Pharm. Med. Chem.* **2002,** 5, 183–186

15. U. Kulandaivelu, V.G. Padmini, K. Suneetha, B. Shireesha, J.V. Vidyasagar, T.R. Rao, A. Basu V. Jayaprakash, *Archiv der Pharmazie*, **2011,***344*, 84-90.

16. E.C. Friedberg, Nature **2003,**421, 436–440.

17. E.C. Friedberg, G.C. Walker, W. Siede, R.D. Wood, eds., American Society for Microbiology Press. **2005,**

18. M.Tascilar, F.A. de Jong, J.Verweij, R.H. Mathijssen, *Oncologist***2006,**11, 732–741.

19. M. Sirajuddin, S. Ali, A. Badshah, *J. Photochem. Photobiol. B: Biol*.**2013,** 124, 1–19.

20. V. Brabec, O. Nováková, *Drug Resist. Updat*. **2006,** 9 (3) 111–122.

21. L.F. Liu, S.D. Desai, T.K. LI, Y. Mao, M.E.I. Sun, S.P. SIM, *Ann. NY. Acad. Sci*.2000. 922, 1–10.

22. R. Martinez, L. Chacon-Garcia, *Curr. Med. Chem*.**2005,**12, 127–151.

23. N. Arshad, N.Abbas, M.H. Bhatti, N.Rashid, M.N.Tahir, S.Saleem, B. Mirza, *J. Photochem. Photobiol. B: Biol*.**2012,**117, 228–239.

24. N. Arshad, S.I. Farooqi, M.H. Bhatti, S. Saleem, B. Mirza, *J.Photochem. Photobiol. B: Biol*. **2013,**125, 70–82.

25. N. Arshad, M. Ahmad, M.Z. Ashraf, H. Nadeem, *J. Photochem. Photobiol. B: Biol*.**2014**, 138, 331–346.

26. N. Arshad, M.H. Bhatti, S.I. Farooqi, S. Saleem, B. Mirza, *Arab. J. Chem.***2016,**9, 451–462.

27. N. Arshad, F. Perveen, A. Saeed, P.A. Channar, S.I. Farooqi, F.A. Larik, H. Ismail, B. Mirza, *J. Mol. Struct*. **2017,** 1139, 371– 380

28. N. Arshad, P.A. Channar, A. Saeed, S.I. Farooqi, A. Javed, F.A. Larik, W.A. Abbasi, U. Flörke, *J. Saudi Chem. Soc.***2018,**22, 1003-1013.

29. S.I. Farooqi, N. Arshad, P.A. Channar, F. Perveen, A. Saeed, F.A. Larik, A. Javeed, *J.Photochem. Photobiol. B: Biol*.**2018**, 189,104–118.

30. A.N. Choudhary, V. Juyal, *Int. J .Pharm. Pharmaceut. Sci.* **2011**, 3,125–128.

31. Bruker SMART (Version 5.63), SAINT (Version 6.02). Bruker AXS Inc., Madison, Wisconsin, USA. **2002.**

32. G.M. Sheldrick, Acta Cryst. **2008,**64, 112–122.

33. M. J.Turner, J. J. McKinnon, S. K. Wolff, D. J. Grimwood, P. R. Spackman, D. Jayatilaka, M. A. Spackman, CrystalExplorer17. The University of Western Australia. **2017.**

34. J. Bernstein, R.E. Davis, L. Shimoni, N.L. Chang, *Chem. Int. Ed. Engl.***1995,**34, 1555–1573.(33)

35. F.L. Hirshfeld, *Theor.Chim. Acta*. **1977**, 44, 129–138.

36. M.A. Spackman, D. Jayatilaka, *Cryst. Eng. Comm.***2009,**11, 19–32.

37. M.A. Spackman, J.J. McKinnon, D. Jayatilaka, Cryst. Eng. Comm**. 2008,**10, 377–388.

38. P. Venkatesan, S. Thamotharan, A. Ilangovan, H. Liang, T. Sundius, *Spectrochim. Acta Part A*, **2016**, 153, 625–636.

39. D. Jayatilaka, D. J. Grimwood, A. Lee, A. Lemay, A. J. Russel, C. Taylor, S. K. Wolff, P. Cassam-Chenai, A. Whitton, **2005.**

40. J.J. McKinnon, D. Jayatilaka, M.A. Spackman, *Chem. Commun*. **2007,** 37, 3814–3816.

41. V.R. Hathwar, M. Sist, M.R. Jørgensen, A.H. Mamakhel, X.Wang, C.M. Hoffmann, K. Sugimoto, J. Overgaard, B.B. Iversen, *IUCrJ*, **2015**, 2 (5) 563–574.

42. N.Raman, R. Mahalakshmi, M. Packiaraj, *Inorg. Chem. Commun*. **2014,** 47, 20–26.

43. N. Shahabadi, A. Fatahi, J. Mol. Struct. **2010,**970 (1-3) 90–95.

44. X.L. Wang, H. Chao, H. Li, X.L. Hong, Y.J. Liu, L.F. Tan, L.N. Ji, *J. Inorg. Biochem.***2004,** 98, 1143–1193.

Figure captions

Fig. 1: Examples of some biological active α-β-unsaturated ketones derivatives.

Fig. 2. The molecular structure of the title compound.

Fig. 3. A partial view of the crystal packing of the title compound. The C—H ··· O and C—H ··· N hydrogen bonds are shown as dashed lines (see Table 2), and only H atoms involved in those interactions have been included for clarity.

Fig. 4. View of the three-dimensional Hirshfeld surface of the title compound plotted over d_{norm} in the range -0.1794 to 1.5932 a.u.

Fig. 5. View of the three-dimensional Hirshfeld surface of the title compound plotted over electrostatic potential energy in the range -0.0500 to 0.0500 a.u. using the STO-3G basis set at the Hartree–Fock level of theory. The C—H ··· O and C—H ··· N hydrogen-bond donors and/or acceptors are viewed as blue and red regions around the atoms corresponding to positive and negative potentials, respectively.

Fig. 6. Hirshfeld surface of the title compound plotted over shape-index.

Fig. 7. The full two-dimensional fingerprint plots for the title compound, showing (a) all interactions, and delineated into (b) H···H, (c) H···C/C···H, (d) H···Br/Br···H, (e) H···O/O···H, (f) C···C, (g) H···N/N···H, (h) N···C/C···N and (i) C···Br/Br···C interactions. The d_i and d_e values are the closest internal and external distances (in Å) from given points on the Hirshfeld surface contacts

Fig. 8. The Hirshfeld surface representations with the function d_{norm} plotted onto the surface for (a) H···H, (b) H···C/C···H, (c) H···Br/Br···H, (d) H···O/O···H, (e) C···C, (f) H···N/N···H, (g) N···C/C···N and (h) C···Br/Br···C interactions.

Fig. 9. The frontier molecular orbital density distribution of **4** after optimization at DFT/ B3LYP/6-31G level. The figure includes optimized structure, electrostatic potential map, bonding molecular orbital (HOMO), anti-bonding molecular orbital (LUMO).

Fig. 10. UV-visible absorption spectrum in the absence and presence of increasing concentrations of ct-DNA from 10 - 90 µM (left) and plot of $A_o/A\text{-}A_o$ vs. $1/[DNA]\ (M)^{-1}$ for the determination of binding constant-K_b and free energy change-ΔG (right).

Fig. 11. Cyclic voltammogram in the absence and presence of increasing concentrations of ct-DNA from 10 – 50 µM (left) and plot of $A_0/A\text{-}A_0$ vs. $1/[DNA](\mu M)^{-1}$ for the determination of binding constant-K_b and free energy change-ΔG (right).

Fig. 12. The plot of relative specific viscosity against Compound–DNA concentrations ratio on adding increasing concentrations of compound (10 – 80 µM) into the fixed concentration of DNA (10µM) at physiological temperature (37 °C).

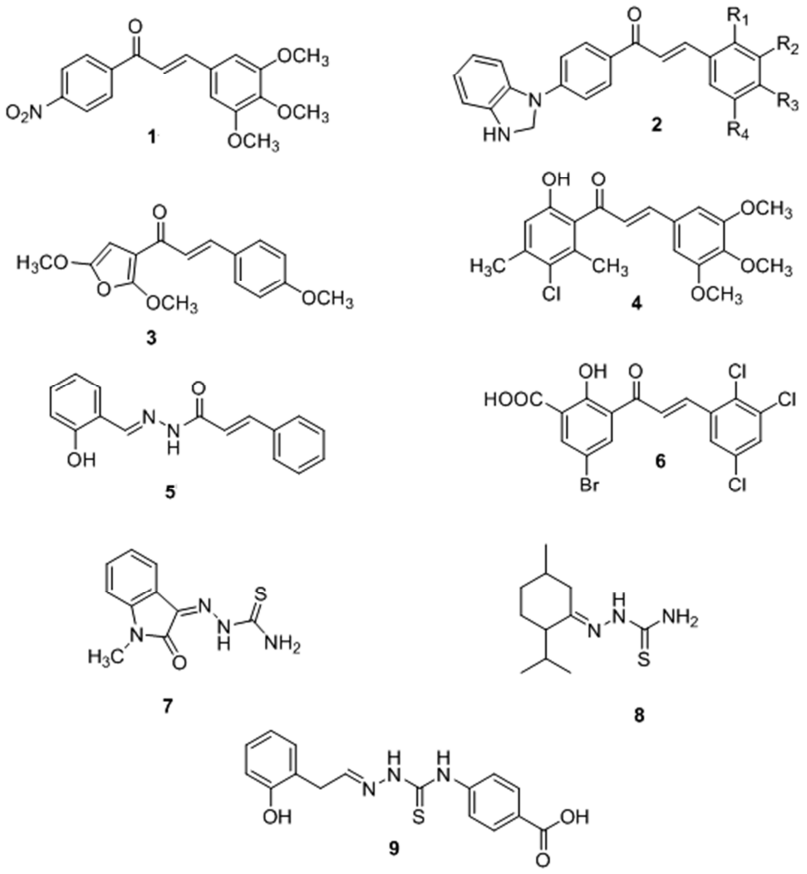

Fig. 1: Examples of some biological active α-β-unsaturated ketones derivatives.

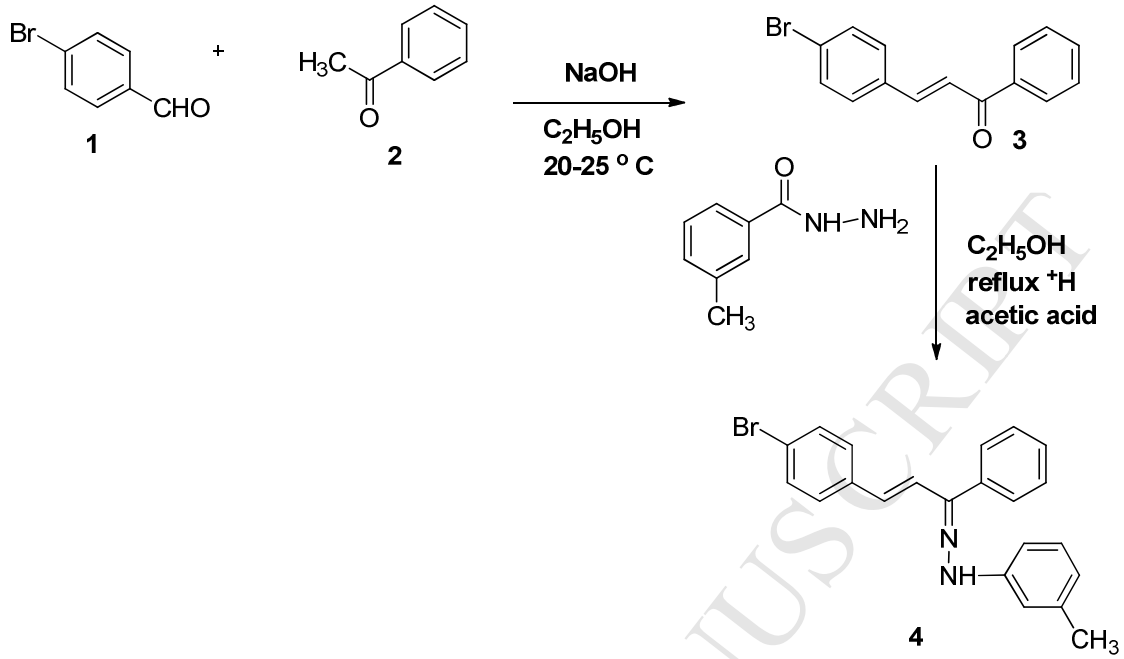

Scheme 1. Synthesis of 1-((E)-3-(4-bromophenyl) -1-phenylallylidene)-2-(m-tolyl)hydrazine.

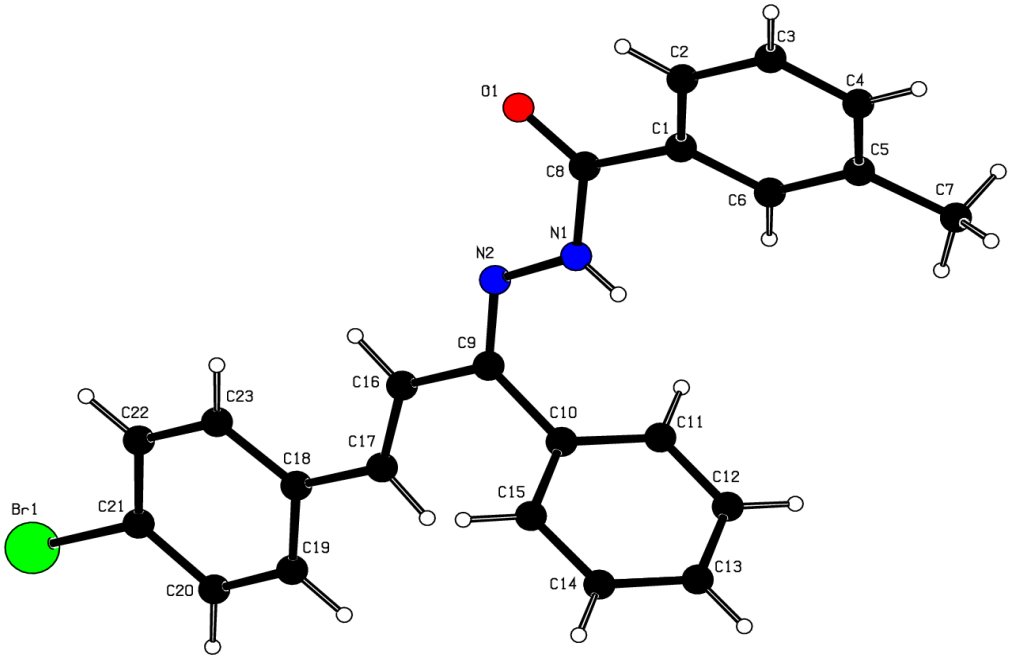

Fig. 2. The molecular structure of the title compound.

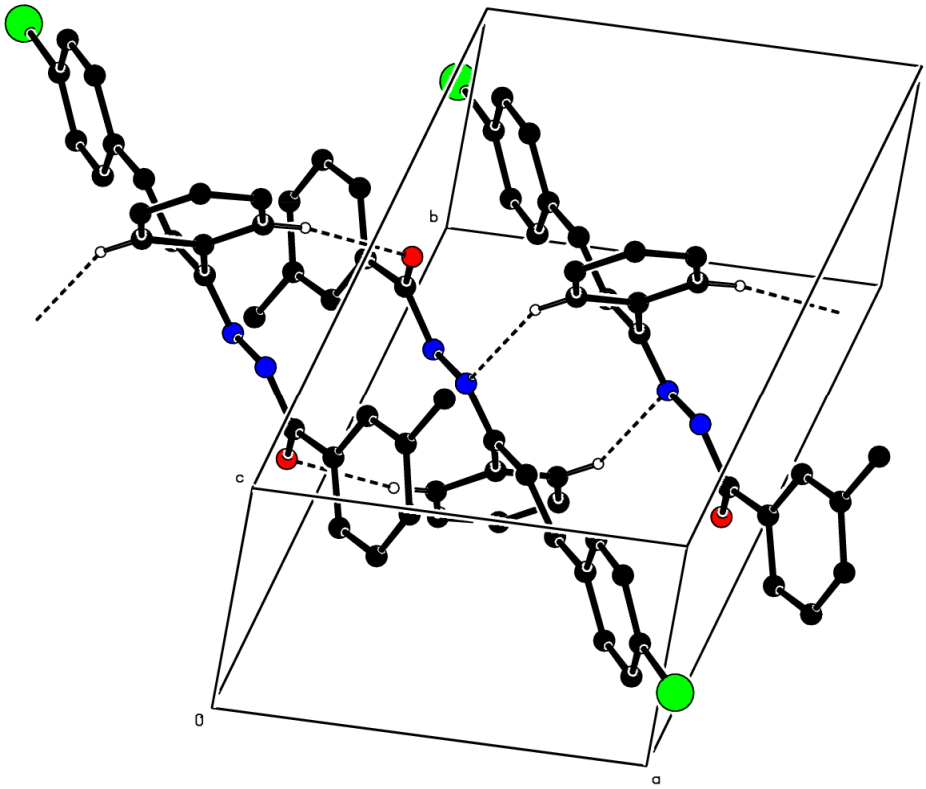

Fig. 3. A partial view of the crystal packing of the title compound. The C—H ··· O and C—H ··· N hydrogen bonds are shown as dashed lines (see Table 2), and only H atoms involved in those interactions have been included for clarity.

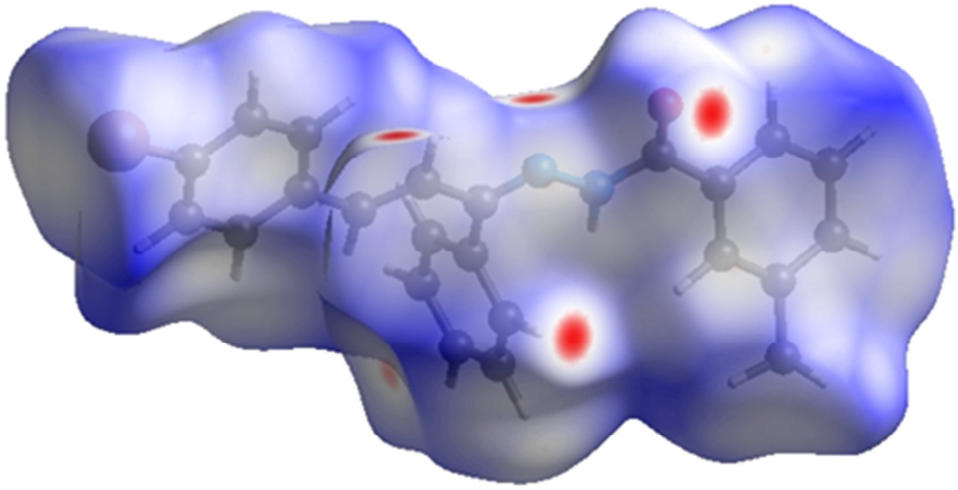

Fig. 4. View of the three-dimensional Hirshfeld surface of the title compound plotted over d_{norm} in the range -0.1794 to 1.5932 a.u.

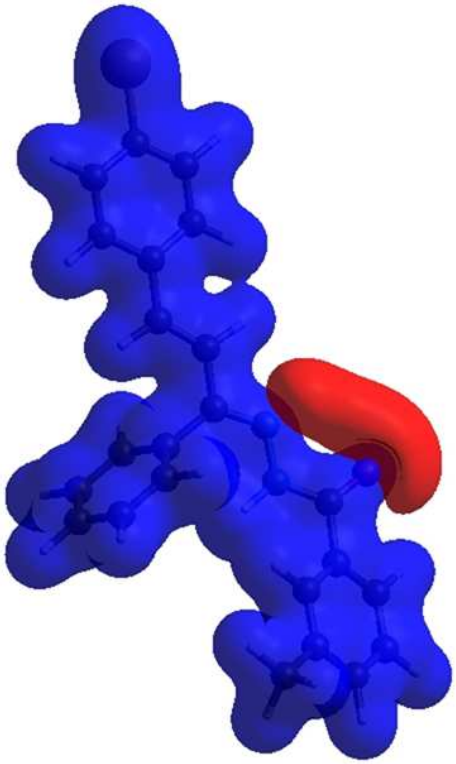

Fig. 5. View of the three-dimensional Hirshfeld surface of the title compound plotted over electrostatic potential energy in the range -0.0500 to 0.0500 a.u. using the STO-3G basis set at the Hartree–Fock level of theory. The C—H ··· O and C—H ··· N hydrogen-bond donors and/or acceptors are viewed as blue and red regions around the atoms corresponding to positive and negative potentials, respectively.

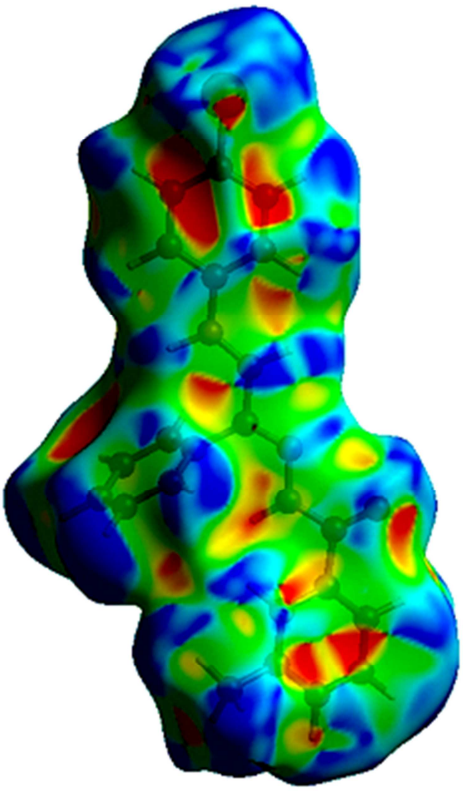

Fig. 6. Hirshfeld surface of the title compound plotted over shape-index.

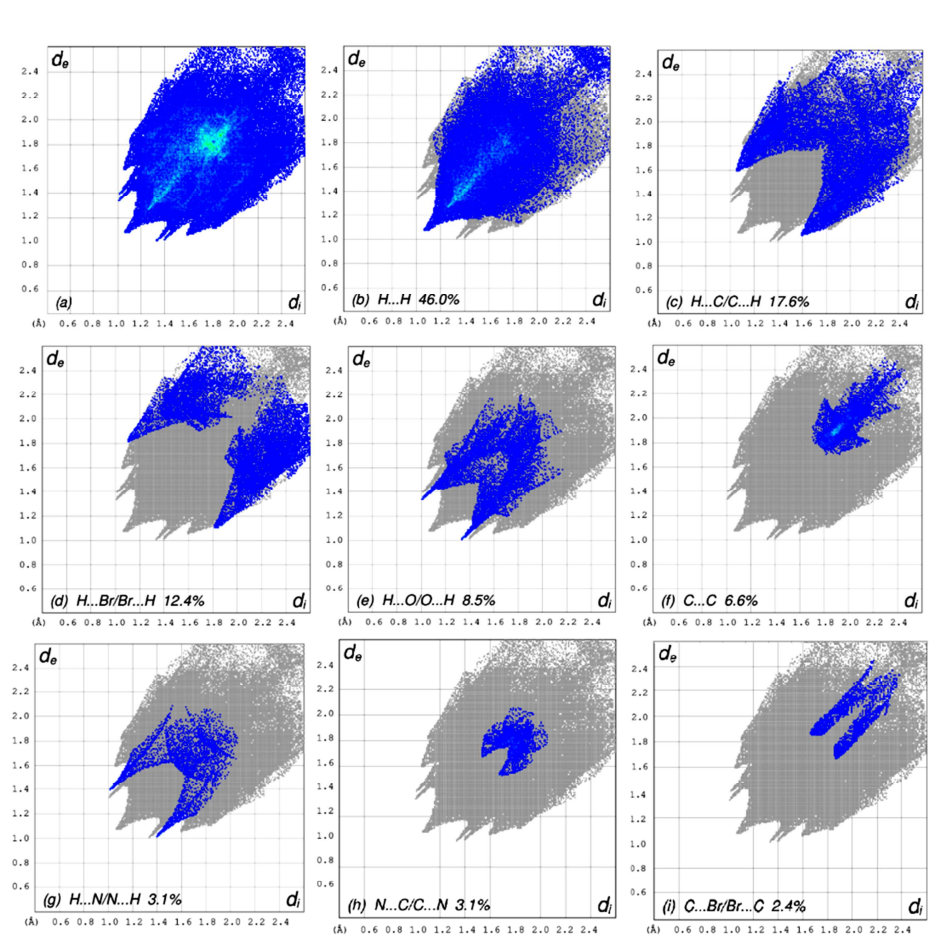

Fig. 7. The full two-dimensional fingerprint plots for the title compound, showing (a) all interactions, and delineated into (b) H···H, (c) H···C/C···H, (d) H···Br/Br···H, (e) H···O/O···H, (f) C···C, (g) H···N/N···H, (h) N···C/C···N and (i) C···Br/Br···C interactions. The d_i and d_e values are the closest internal and external distances (in Å) from given points on the Hirshfeld surface contacts

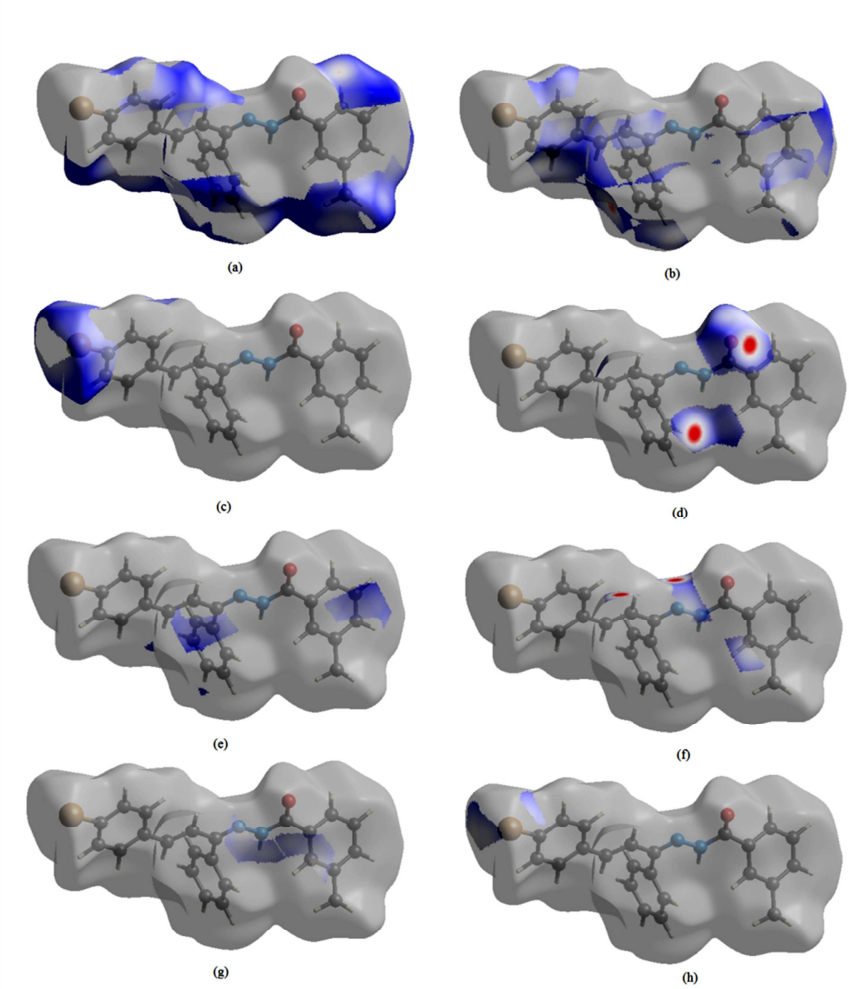

Fig. 8. The Hirshfeld surface representations with the function d_{norm} plotted onto the surface for (a) H···H, (b) H···C/C···H, (c) H···Br/Br···H, (d) H···O/O···H, (e) C···C, (f) H···N/N···H, (g) N···C/C···N and (h) C···Br/Br···C interactions.

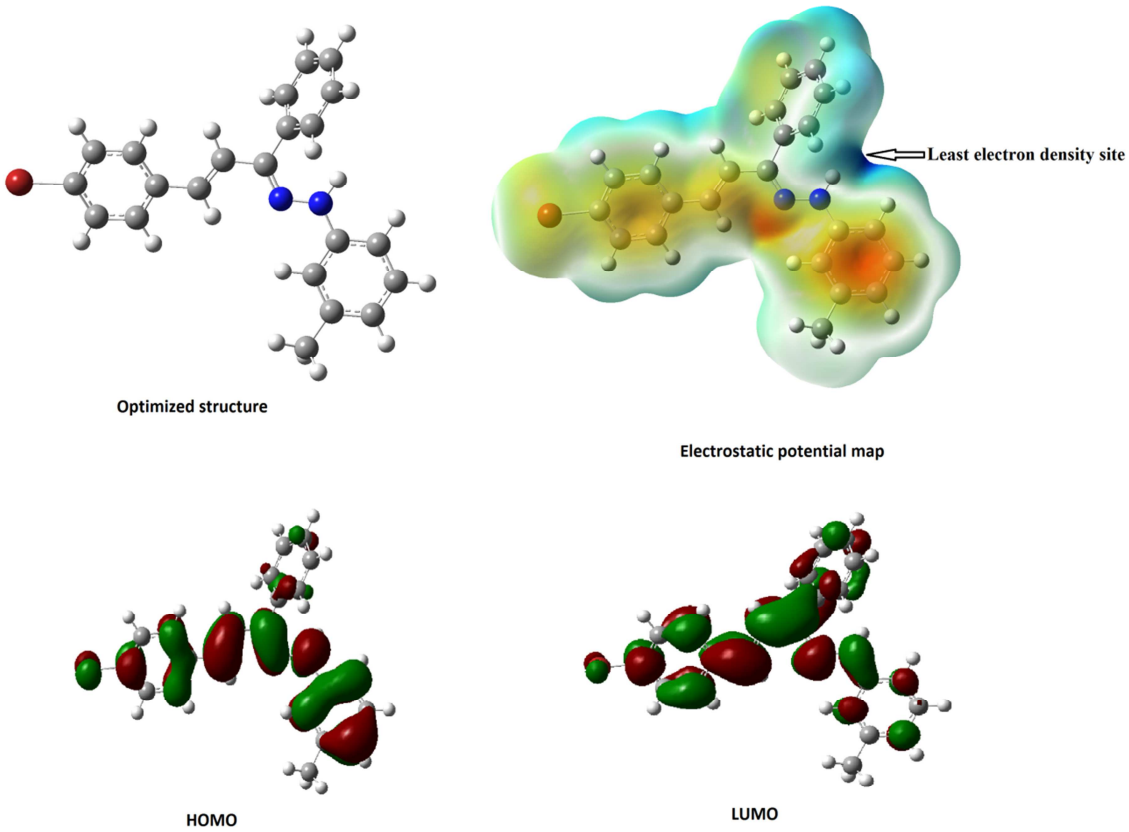

Fig. 9. The frontier molecular orbital density distribution of **4** after optimization at DFT/ B3LYP/6-31G level. The figure includes optimized structure, electrostatic potential map, bonding molecular orbital (HOMO), anti-bonding molecular orbital (LUMO).

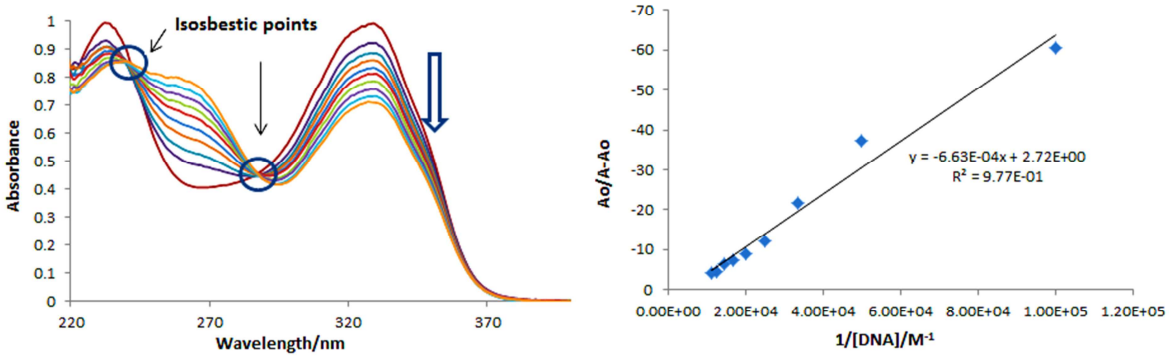

Fig. 10. UV-visible absorption spectrum in the absence and presence of increasing concentrations of ct-DNA from 10 - 90 µM (left) and plot of $A_o/A\text{-}A_o$ vs. 1/[DNA] $(M)^{-1}$ for the determination of binding constant-K_b and free energy change-ΔG (right).

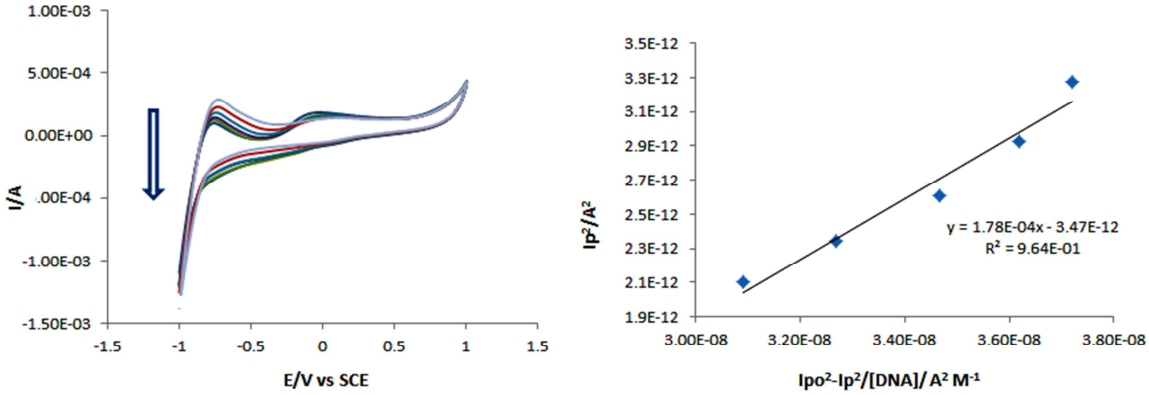

Fig. 11. Cyclic voltammogram in the absence and presence of increasing concentrations of ct-DNA from 10 – 50 µM (left) and plot of $A_0/A\text{-}A_0$ vs. $1/[DNA](\mu M)^{-1}$ for the determination of binding constant-K_b and free energy change-ΔG (right).

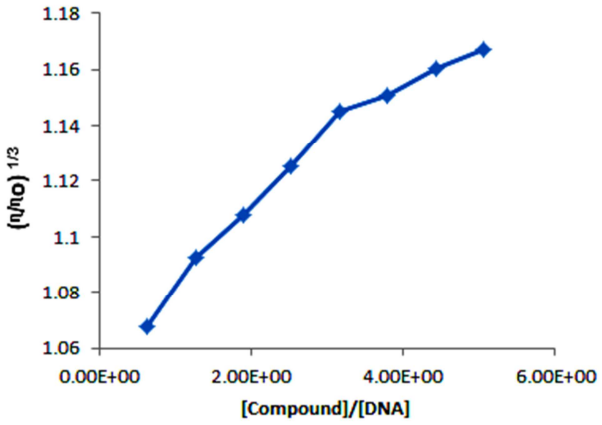

Fig. 12. The plot of relative specific viscosity against Compound–DNA concentrations ratio on adding increasing concentrations of compound (10 – 80 µM) into the fixed concentration of DNA (10µM) at physiological temperature (37 °C).

Table 1
Experimental details for the title compound.

Empirical formula	$C_{23}H_{19}BrN_2O$	
Formula weight	419.31	
Temperature	130(2) K	
Wavelength	0.71073 Å	
Crystal system	triclinic	
Space group	P -1	
Unit cell dimensions	a = 8.629 (2) Å	α= 70.179(5)°
	b = 10.489 (3) Å	β= 88.988(5)°
	c = 12.171 (3) Å	γ = 71.450(5)°
Volume	977.4 (4) $Å^3$	
Z	2	
Densitiy (calculated)	1.425 Mg m^{-3}	
Absorbtion cocfficient	2.117 mm^{-1}	
F (000)	428	
Crystal size	0.28 × 0.18 × 0.13 mm^3	
Θ range for data collection	1.79-27.88°	
Index ranges	$-11 \le h \le 11$, $-13 \le k \le 13$, $-15 \le l \le 15$	
Absorption correction	Semi-empirical from equivalents	
T_{min} / T_{max}	0.7704 / 0.5886	
Reflections collected	9172	
Independent reflections	4638 [R(int) = 0.0318]	
Refinement method	Full-matrix least-squares on F^2	
Data/restraints/parameters	4638/0/249	
Goodness-of-fit on F^2	0.984	
Final *R* indices	R_1 = 0.0391	
[$I > 2\sigma(I)$]	wR_2 = 0.0835	
R indices (all data)	R_1 = 0.0588	
	wR_2 = 0.0892	
Largest diff. peak and hole (e $Å^{-3}$)	0.596 / -0.270	

Table 2

Hydrogen-bond geometry (Å, ^{o}) for the title compound.

D-H···A	**D-H**	**H···A**	**D···A**	**D-H···A**
C11—H11A···O1^{iv}	0.95	2.50	3.438(3)	171
C15—H15A···N2^{v}	0.95	2.55	3.421(3)	153

Symmetry codes: (iv) −x+2, −y+1, −z+1; (v) −x+1, −y+1, −z+1.

Table 3

The selected interatomic distances (Å).

Br1···C12[i]	3.615 (2)	C12···C20[vi]	3.585 (4)
Br1···C13[i]	3.559 (3)	C15···C17	3.348 (3)
Br1···C14[ii]	3.728 (3)	H1···C6	2.58 (3)
O1···N2	2.717 (3)	H1···C10	2.44 (3)
O1···C19[iii]	3.353 (3)	H1···C11	2.54 (3)
O1···H11A[iv]	2.50	H1···H6A	2.17
N1···C11	3.084 (3)	H1···H11A	2.52
N2···C6[iv]	3.233 (3)	H2A···H19A[iii]	2.41
N2···C1[iv]	3.384 (3)	H14A···Br1[ii]	3.03
N2···C15[v]	3.421 (3)	H4A···H7B	2.60
N2···C16[v]	3.430 (3)	H6A···H7C	2.36
N1···H6A	2.60	H16A···H23A	2.15
N2···H15A[v]	2.55	H17A···H19A	2.41
C2···C19[v]	3.508 (4)	C8···C18[v]	3.596 (4)
C2···C20[v]	3.527 (4)	C9···C9[v]	3.569 (4)
C8···C17[v]	3.568 (4)		

Symmetry codes: (i) x−1, y+1, z−1; (ii) −x, −y+2, −z+1; (iii) x+1, y−1, z; (iv) −x+2, −y+1, −z+1; (v) −x+1, −y+1, −z+1; (vi) −x+1, −y+2, −z+1.

Table 4

Selected bond lengths (Å), bond and torsion angles (º) for the title compound.

Parameters	***X-ray analysis***
The bond lenghts (Å)	
Br1 — C21	1.902 (2)
O1 — C8	1.222 (3)
N1 — N2	1.365 (3)
N1 — C8	1.374 (2)
N2 — C9	1.299 (3)
C1—C8	1.485 (3)
C9 — C16	1.450 (3)
C16—C17	1.339 (3)
C17—C18	1.460 (3)
The bond angles (º)	
N2—N1—C8	119.94 (18)
C9—N2—N1	117.38 (18)
O1—C8—N1	122.5 (2)
O1—C8—C1	123.32 (19)
N1—C8—C1	114.22 (19)
N2—C9—C16	114.41 (19)
N2—C9—C10	124.54 (19)
C20—C21—Br1	119.42 (17)
C22—C21—Br1	119.27 (17)
The torsion angles (º)	
C8—N1—N2—C9	177.2 (2)
N2—N1—C8—O1	−5.7 (3)
N2—N1—C8—C1	174.29 (19)
C2—C1—C8—O1	−27.0 (3)
C6—C1—C8—O1	150.0 (2)
C2—C1—C8—N1	153.0 (2)
C6—C1—C8—N1	−30.0 (3)
N1—N2—C9—C16	178.57 (18)
N1—N2—C9—C10	−2.4 (3)
N2—C9—C10—C15	−112.9 (3)
N2—C9—C10—C11	65.3 (3)
C19—C20—C21—Br1	−178.52 (18)
Br1—C21—C22—C23	178.85 (18)

Table 5

Computed parameters of compound **4** by DFT (B3LYP/6-31G level).

Parameters	Computed values
E_{Homo}(ev)	-0.18301
E_{Lumo}(ev)	-0.06349
ΔE (eV)	0.11952
Ionization potential (eV)	0.18301
Electron affinity (eV)	0.06349
Binding energy (a.u)	-3530.6
Dipole moment (D)	4.07
Electronegativity (X)	0.12325
Global hardness (H)	0.067
Point group	C_1